Life Sciences 355 (2024) 122992

Contents lists available at ScienceDirect

Life Sciences

journal homepage: www.elsevier.com/locate/lifescie

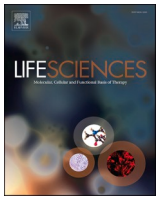

A novel bioprinted microtumour model for studying acute-leukemia-cell-contaminated in ovarian tissue

Saeid Moghassemi [1], Arezoo Dadashzadeh [1], Christiani A. Amorim [*]

Pôle de Recherche en Physiopathologie de la Reproduction, Institut de Recherche Expérimentale et Clinique, Université Catholique de Louvain, Brussels, Belgium

ARTICLE INFO

Keywords:
Alginate
Bioprinting
Cancer therapy
Fibrin
Hydrogel
Tissue engineering

ABSTRACT

Microtumor models, combining cancer and stromal cells within 3D hydrogels, are vital for testing anticancer therapies. Bioprinting hydrogel scaffolds allows tailored *in vitro* models. We created a 3D microtumor model using a bioprinter, with varying ratios of ovarian stromal cells and leukemia cells (HL-60). PEGylated fibrinogen and alginate hydrogel were used. Cell dynamics and proliferation were assessed *via* immunofluorescence staining. Microtumors with different HL-60 ratios (1:1, 1:10, 1:100) were cultured for 5 days. Results showed tumor development modulation by cell ratios and culture time. A significant cell density increase occurred in 1:1 ratio microtumors, indicating rapid cancer cell proliferation. No HL-60 cells were found in 1:100 ratio microtumors by day 5. The 1:10 ratio closely mimicked leukemia invasion in ovarian tissue, showing detectable cancer cells by days 3 and 5 without altering total cell density dynamics significantly. This bioprinted leukemia microtumor model offers better physiological relevance than 2D assays, promising applications in cellular analysis and drug screening.

1. Introduction

Nowadays, one of the most pragmatic approaches for generating realistic *in vitro* microtumor models is through 3D bioprinting of hydrogel-based biomaterial scaffolds [1]. This innovative technique facilitates the precise placement of cell-laden bioinks into intricate structures, guided by computer-aided design files with exceptional accuracy, efficiency, and reproducibility. Specifically in tumor modeling, bioprinting offers unparalleled precision in embedding cancer cells within hydrogels containing healthy cell populations, thus mimicking the intricate milieu of the tumor microenvironment (TME) [2]. Leveraging their inherent structural complexity, essential for fostering dynamic cell-cell and cell-matrix interactions, 3D bioprinted models have become indispensable tools in numerous areas of cancer research [3,4].

Leukemia is one of the most prevalent cancer types among prepubertal girls and women of reproductive age, exhibiting one of the highest rates of ovarian metastases [5,6]. Despite advancements in cancer therapies contributing to a notable survival rate among patients, these treatments can potentially affect fertility and ovarian function [7,8]. While autotransplantation of cryopreserved ovarian tissue presents a promising option for restoring endocrine and reproductive functions, it is not advised for leukemia patients due to the considerable risk of disease recurrence [5]. One of the most recent methods being developed to restore fertility in these individuals safely involves purging ovarian tissue fragments of cancer cells before autotransplantation [9,10]. However, the scarcity and precious nature of ovarian fragments from leukemia patients pose significant challenges for research and development efforts in this area [11].

In this study, we have devised a novel bioink comprising a blend of proprietary fibrinogen and alginate to mimic leukemia cell invasion into ovarian tissue, thereby creating a tumor-infiltration mimicking model (TIM) for drug development applications. To achieve this goal, we optimized the HL-60:SCs cell ratio to (i) prevent solid tumor formation, as leukemia cells are generally found in body fluids, characterized as liquid tumors, and (ii) ensure adequate presence of cancer cells for detection by common analyses, like immunofluorescence, thereby establishing a realistic model. The TIMs' preparation was executed using a bioprinter equipped with state-of-the-art microfluidic technology.

* Corresponding author at: Pôle de Recherche en Physiopathologie de la Reproduction, Institut de Recherche Expérimentale et Clinique, Université Catholique de Louvain, Avenue Hippocrate 54, bte B1.55.03, 1200 Brussels, Belgium.
E-mail address: christiani.amorim@uclouvain.be (C.A. Amorim).
[1] These authors contributed equally to this work.

https://doi.org/10.1016/j.lfs.2024.122992
Received 30 May 2024; Received in revised form 26 July 2024; Accepted 13 August 2024
Available online 16 August 2024

2. Methods

2.1. Ovarian stromal cell isolation and in vitro culture

Ovarian stromal cells (SCs) were isolated [12,13] from frozen-thawed ovarian tissue fragments [14] following approval by the Institutional Review Board of the University Catholique de Louvain on May 23, 2019 (IRB reference 2018/19DEC/475). Briefly, frozen-thawed ovarian biopsies [15], obtained from three postmenopausal multi-organ donors. They were first mechanically minced using a tissue chopper (McIlwain, Campden Instruments, Loughborough, UK), and the resulting fragments were then enzymatically digested using 0.28 Wünsch units/ml Liberase DH (5,401,054,001, Sigma), and 8 Kunitz units/ml DNase (10,104,159,001, Sigma) for 75 min at 37 °C. To inactivate the enzymatic activity, Dulbecco's phosphate-buffered saline without Ca^{2+} and Mg^{2+} (DPBS; 14,190,144, Gibco) supplemented with 10 % heat-inactivated fetal bovine serum (HI FBS; 16,140–071, Gibco) was added to the suspension in equal proportions. To remove the last few particles, the suspension was subsequently filtered through 80 μm (NY8002500, Millipore, Sigma) and 30 μm (NY3002500, Millipore, Sigma) nylon net filters. The final suspension underwent centrifugation (500 *g*, 10 min), and the pellet was resuspended in cell culture media Dulbecco's modified of Eagle's medium F-12 nutrient mixture (DMEM/F12; 21,041–025, Gibco), 10 % HI FBS and 1 % antibiotics and antimycotic (AA; 15,240–062, Gibco) were cultured in a T75 culture flask.

2.2. Leukemia cell culture

HL-60 cell line (98,070,106, Sigma) was cultured in T75 culture flasks, using RPMI medium (61870–010, Gibco) supplemented with 10 % HI FBS, and 1 % AA and under humidified conditions with 5 % CO_2 at 37 °C.

2.3. Bioink preparation

PEGylate fibrinogen (PF) with the molar ratio of PEG: Fib 20:1 was prepared to formulate the bioink. Human fibrinogen was dissolved in PBS to a concentration of 85 mg/ml, then filtered through a 0.22 mm syringe filter and incubated at 37 °C. Then, an equal volume of prewarmed fibrinogen was combined with a 10 mg/ml NHS-PEG-NHS solution and incubated at 37 °C for 2 h. Moreover, 1.12 % alginate was prepared by dissolving alginate (9842, Aspect Biosystems) in PBS overnight at 4 °C. This alginate solution was combined with PF at a concentration of 47.5 mg/ml and mixed with HL-60:SCs cells (1×10^6 cells/ml) at a ratio of 1:1, 1:10, or 1:100 (shell A1, shell A2, or shell A3, respectively), resulting in final concentrations of 1 % alginate and 5 mg/ml PF. Moreover, 1.12 % alginate was diluted with PBS to achieve an alginate concentration of 0.5 % (shell B) to provide support for shell A. During printing, CAT-2™ (0458, Aspect Biosystems) containing polyvinyl alcohol and $CaCl_2$ was used for crosslinking, while sodium chloride solution, (0460, Aspect Biosystems) was used to flush the channels of the printhead. All the experiments were performed in triplicate.

2.4. TIMs bioprinting process

A pneumatic microfluidic bioprinter (RX1, Aspect Biosystems) was utilized to print the bioink, operating *via* air pressure to regulate valve openings and reservoir flows. The Centra™ printhead, capable of printing two different shells, two cores, a crosslinker, and a buffer, was integrated into the bioprinter (Fig. 1) [16]. During bioprinting, the crosslinker surrounding the bioink initiates primary physical crosslinking, resulting in filament formation ejected from the printhead nozzle. In the bioprinter software, a rectangular volume of $1 \times 10 \times 10$ mm with 5 % infill was configurated, and the scaffold was deposited onto mesh paper with printing pressures set at 105,43, 200, and 150 mbar for shell A, shell B, crosslinker, and buffer, respectively. Parameters, such as the nozzle-to-mesh paper, printing speed, and row speed, were set at 6 mm, 11 mm/s, and 11 mm/s, respectively. After printing, the bioprinted scaffolds underwent post-printing crosslinking with 40 mM $CaCl_2$ for 15 min at room temperature, along with 5 IU/ml thrombin included in the culture medium composed of DMEM-F12, 10 % HI FBS, and 1 % AA. (See Table 1.)

2.5. LIVE/DEAD assay

Cell viability within the bioink pre- and post-printing was evaluated using the LIVE/DEAD™ Viability/Cytotoxicity test (L3224, Invitrogen, Thermo Fisher) [10]. Briefly, the bioinks were treated for 30 min at

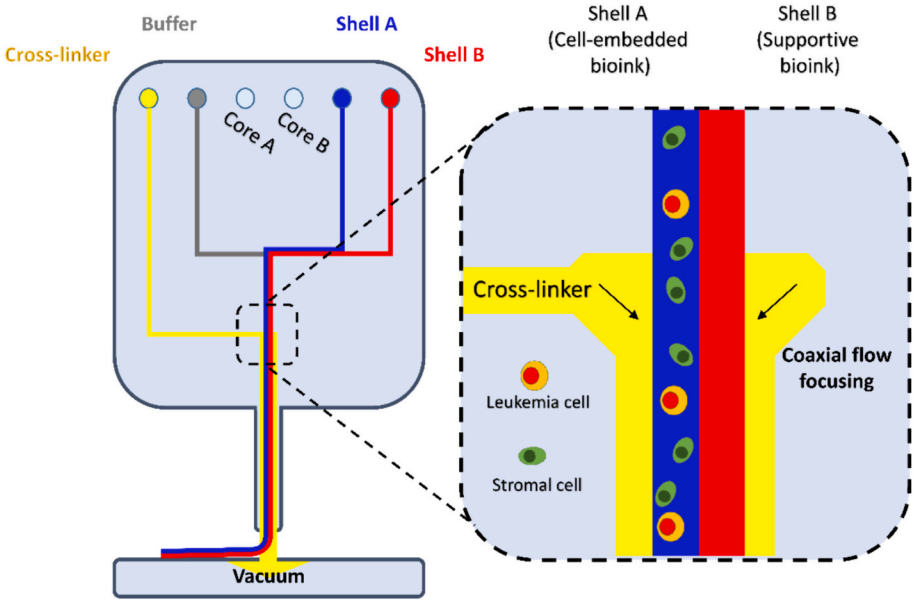

Fig. 1. Schematic illustration of the reaction between the bioink and cross-linker in the Aspect Biosystems' Lab-On-a-Printer microfluidic printhead. To reduce the shear stress that cells suffer when the bioink exits the nozzle and is applied to the print bed, a printable gel is introduced into the printhead's nozzle and sheathed on each side by cross-linkers.

Table 1
Cell density of TIMs with different ratios of HL-60:SCs on days 0, 3, and 5.

Combination (Hl-60:SCs)	Cell density (cells per mm^2)			Cell density dynamics (%)	
	Day 0	Day 3	Day 5	Day 3	Day 5
1:1	269.23 ± 38.46 [a]	634.62 ± 96.15	826.92 ± 134.62 [a]	57.52 ± 0.38	67.33 ± 0.67
1:10	269.23 ± 76.92	461.54 ± 115.38	557.69 ± 19.23	42.22 ± 2.22	52.14 ± 12.14
1:100	307.69 ± 76.92	442.31 ± 134.62	538.46 ± 76.92	29.17 ± 4.17	43.75 ± 6.25

The letter in the same row indicates the statistical difference ($p < 0.05$).

37 °C in the dark in DPBS with 2 mmol/l calcein-AM and 5 mmol/l ethidium homodimer-I. Calcein-AM, a non-fluorescent cell-permeant dye, penetrates living cells and is cleaved by esterases to yield calcein, producing intense and consistent green fluorescence within viable cells. Bright red fluorescence upon ethidium homodimer-I penetration and binding to DNA *via* damaged membranes. Then, cell viability was examined using an inverted fluorescence microscope (Leica DMIL).

2.6. Degradation study

The *in vitro* degradation of the hydrogels was assessed using the gravimetric technique [17,18]. Bioprinted hydrogels were initially prepared, post-bioprinted, by immersion in a $CaCl_2$ solution for 15 min, followed by submersion in either DMEM/F12 of PBS containing 5 IU/ml thrombin for 2 h at 37 °C. Then, the bioprinted hydrogels were meticulously weighed after being dried three times on lint-free tissue papers and then submerged again in media (DMEM/F12 or PBS solution, pH 7.4, 0.01 M, containing 0.1 % sodium azide). The hydrogels were removed and weighed every 24 h after excess surface water was eliminated ($n = 4$). Fresh media were replenished every other day, and the percentage remaining mass of the samples was calculated using the flowing equation:

$$\text{Percentage remaining mass} = (Wn/W0) \times 100 \quad (1)$$

where Wn represents the weight of the bioprinted hydrogel after n days of culturing and W0 is the initial weight of the hydrogel immediately after exposure to post-printing crosslinkers.

2.7. Histological study

Before and either 3 or 5 days after culturing, TIMs were fixed in a 4 % formaldehyde solution and embedded in paraffin. Subsequently, sections with a thickness of 7 μm were cut and mounted on microscopic slides. Hematoxylin and eosin (Hx61057849 and Hx87833544, Sigma) staining was performed for morphological analysis. The total cell density was evaluated within a 200 × 200 μm^2 area using ImageJ and the following equation was used to determine the cell density dynamic after 3 or 5 days [12].

$$\text{Cell density dynamic} = (CDn - CD0)/CDn \times 100 \quad (2)$$

where CDn represents the cell density on day 3 or 5, and CD0 is the cell density on day 0.

2.8. Immunofluorescence analysis

Sections were mounted on Menzel-Glaser's Superfrost Plus slides. CD43/Ki-67 practical immunofluorescence analysis was conducted to assess cell proliferation and cancer cell identification simultaneously [6,19]. Histosafe (Yvsolab SA, Turnhout, Belgium) and isopropanol were used for deparaffinization and rehydration of sections, respectively. Then, after demasking sections with citrate buffer and Triton X-100 (X100; for 20 min microwave, the non-specific binding sites were blocked by incubation with TBS/Tween (663684B; VWR) solution containing 10 % normal goat serum (NGS; 31,872, Invitrogen) and 1 % bovine serum albumin (BSA; 3854.3, Karl Roth) for 30 min. Afterward, the sections were then incubated overnight at 4 °C with the polyclonal CD43 antibody (1:150) (1-CD160; Quartett GmbH). Then, the slides were subsequently incubated for 40 min with Alexa Fluor™ 488 goat anti-mouse IgG (A11001, Invitrogen). After another antigen retrieval, the slides were incubated overnight at 4 °C with the monoclonal anti-human Ki67 (1:90) (M7240; DAKO) and 40 min with Alexa Fluor™ 594 goat anti-mouse IgG (A11005, Invitrogen). After staining with Hoechst 33342 (14,533, 1:500, Sigma), sections were mounted with fluorescent mounting medium (S3023; Dako) on glass slides and scanned using an automatic slide scanner (ZEISS Axio Scan.Z1) equipped with three laser lines of 455, 488, and 594 nm. Using ZEN Blue, the HL-60 and SC cell densities were evaluated within a 180 × 180 μm^2 area. Eq. (2) was used to determine the cell density dynamics after 3 or 5 days ($n = 5$). The HL-60 cell proportion was calculated using the following equation:

$$\text{HL} - 60 \text{ cell proportion } (\%) = N_{CD43}/N_T \times 100 \quad (3)$$

where N_{CD43} represents the number of CD43-positive cells within a 180 × 180 μm^2 area, and N_T is the total number cell.

2.9. Statistical analysis

For the statistical analysis of the quantitative data, one-way ANOVA was employed and was presented as mean ± SD. Statistics were considered significant for P values <0.05 and the error bars in graphs reflect a single sample standard deviation.

3. Results

3.1. Assessment of cell survival in bioprinted TIMs

The innovative TIM, containing HL-60 and SCs, was designed using a computer-aided design file (Fig. 2a) and generated using the RX1 Bioprinter. Fig. 2b illustrates an example of the TIM structure stained with polybead microspheres after printing. Shear stress on cells within the bioink during extrusion from the printing nozzle is a primary concern in bioprinting research, potentially leading to cell death [20]. However, the microfluidic technology integrated into the Aspect Biosystems RX1 printhead effectively minimizes the shear stress. LIVE/DEAD assay on the cell-embedded bioink before and immediately after printing demonstrated no significant difference in viability, with high viability rates of 96.15 ± 1.41 and 94.93 ± 2.63, respectively (Fig. 2c,d).

3.2. Evaluation of the degradation in bioprinted hydrogels

The degradation behaviors of bioprinted scaffolds in different media are presented in Fig. 3. On days 1 and 2, hydrogels in both PBS and DMEM/F12 showed similar remaining mass percentages. However, hydrogels in DMEM/F12 continue to maintain their mass until the fifth day, showing no significant difference. In contrast, bioprinted constructs in PBS started to undergo dramatic degradation from the third day onwards and were no longer found in the plates by day 5. The remaining mass of hydrogels in DMEM/F12 of >100 % indicates the swelling of hydrogels and the swollen filaments can be observed in the presentative degradation pictures (Fig. 3).

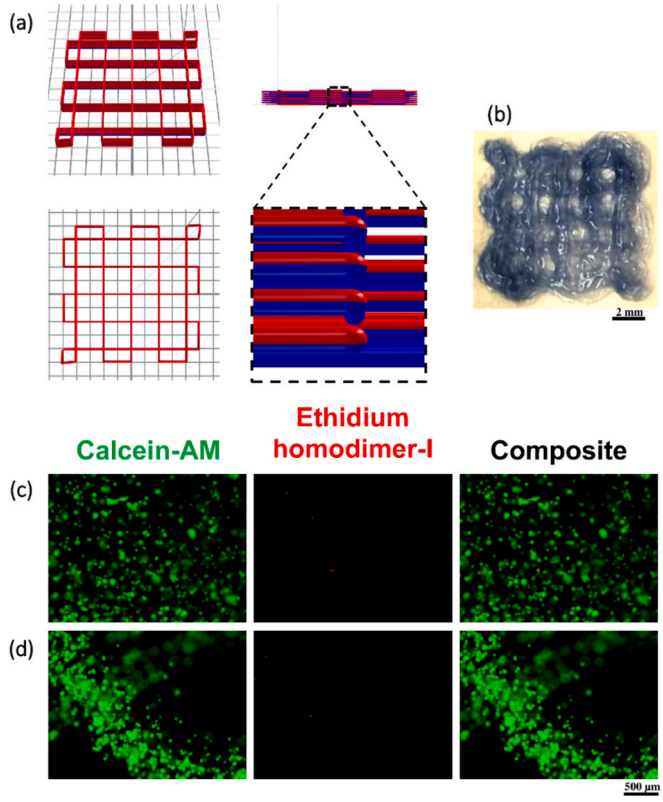

Fig. 2. Innovative TIM development following a computer-aided design file (a) (grid line: 1 mm) and an example of the TIM structure (b). LIVE/DEAD assay on the cell-embedded bioink before (c) and after (d) printing process.

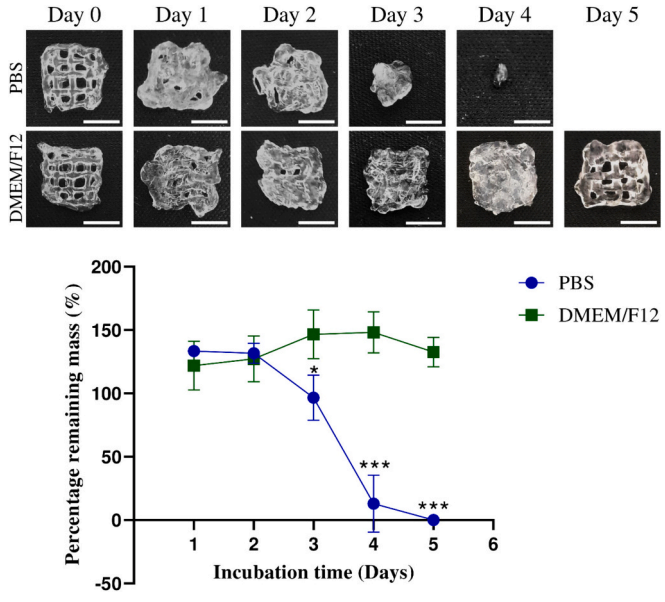

Fig. 3. Degradation behavior of bioprinted hydrogel during a 5-day incubation in PBS and DMEM/F12Degradation profiles (a) (scale bar: 5 mm) and its profile (b) (*, $P < 0.05$; ***, $P < 0.001$).

3.3. Analysis of cell density and morphology of printed cells

The bioprinted hydrogels containing HL-60 and SCs were cultured for 5 days. To examine cell morphology, cell density within the hydrogels, and the dynamics of cell density, samples were fixed on days 0, 3, and 5 and assessed by the histological analysis (Fig. 4). Initially, no

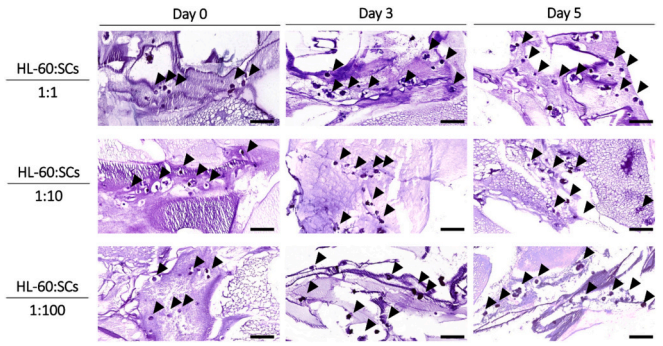

Fig. 4. Histological analysis of TIMs with different ratios of HL-60:SCs (1:1, 1:10, and 1:100) on days 0, 3, and 5 (scale bar: 100 μm).

significant difference was observed in the cell density between different groups on the first day. However, TIMs with an HL-60:SCs ratio of 1:1 showed a significant increase in cell density on the fifth day compared to day 0, demonstrating the highest cell density dynamic. Moreover, no significant differences were observed in cell density or cell density dynamics between the groups with HL-60:SCs ratios of 1:10 and 1:100 after different days of culturing.

3.4. Development of bioprinted TIMs

To evaluate the HL-60:SCs cell ratio in different groups, immunofluorescence analysis has been employed to distinguish healthy cells from cancer cells and simultaneously assess cell proliferation (Fig. 5a). As indicated by the quantified cell proportion graphs (Fig. b-d), different groups showed different levels of HL-60 contamination on the third and fifth days. Notably, no cancer cells could be detected in the TIMs with the HL-60:SCs cell ratio of 1:100 after 5 days of incubation. While the TIMs with a 1:1 cells ratio demonstrated a proliferation rate of 43.09 ± 15.31 % for HL-60 cells after 5 days of incubation, the proliferation rate of SCs was only 2.08 ± 2.95 %, marking the lowest rate among SCs in different groups (Fig. 5e-g). Table 2 illustrates the cell density dynamic of SCs and HL-60 in different groups on the third and fifth days. The results demonstrate a considerable difference between the cell density dynamics of SCs and HL-60 in the 1:1 cell ratio group on day 5, indicating that the significant increase in total cell density was attributable to the high proliferation speed of cancer cells. Moreover, the cell density dynamics of the 1:10 cell ratio group remained stable over time.

4. Discussion

Bioprinting of hydrogel-based biomaterials has been successfully employed to create tumor models for various cancer types, such as glioblastoma [21], cervical tumor [22], and breast cancer [23]. In this study, the bioprinted hydrogels comprised alginate as the primary biomaterial along with a low concentration of PEGylated fibrinogen. Alginate, a natural polysaccharide, undergoes physical crosslink in the presence of divalent cations such as Ca^{2+}, which can slowly release in a Ca^{2+}-free medium, leading to alginate dissolution [24]. The addition of $CaCl_2$ in the printing crosslinking solution triggers the initial physical crosslinking of alginate, generating a filament from the microfluidic nozzle. Post-printing, $CaCl_2$ further enhances the mechanical properties of the printed structure. PEGylation is a chemical reaction that improves protein stability and shields against protease activity [12]. Thrombin in the medium polymerizes PF by cleaving fibrinogen, and Ca^{2+} in the scaffold further stabilizes the PF network. The RX1 bioprinter provides printing of different materials and simultaneous printing of bioinks and the crosslinker by using a microfluidic printhead. Bioinks surrounded by crosslinker experience less shear stress compared to printing bioinks alone, providing an appropriate system for bioprinting sensitive cells [25].

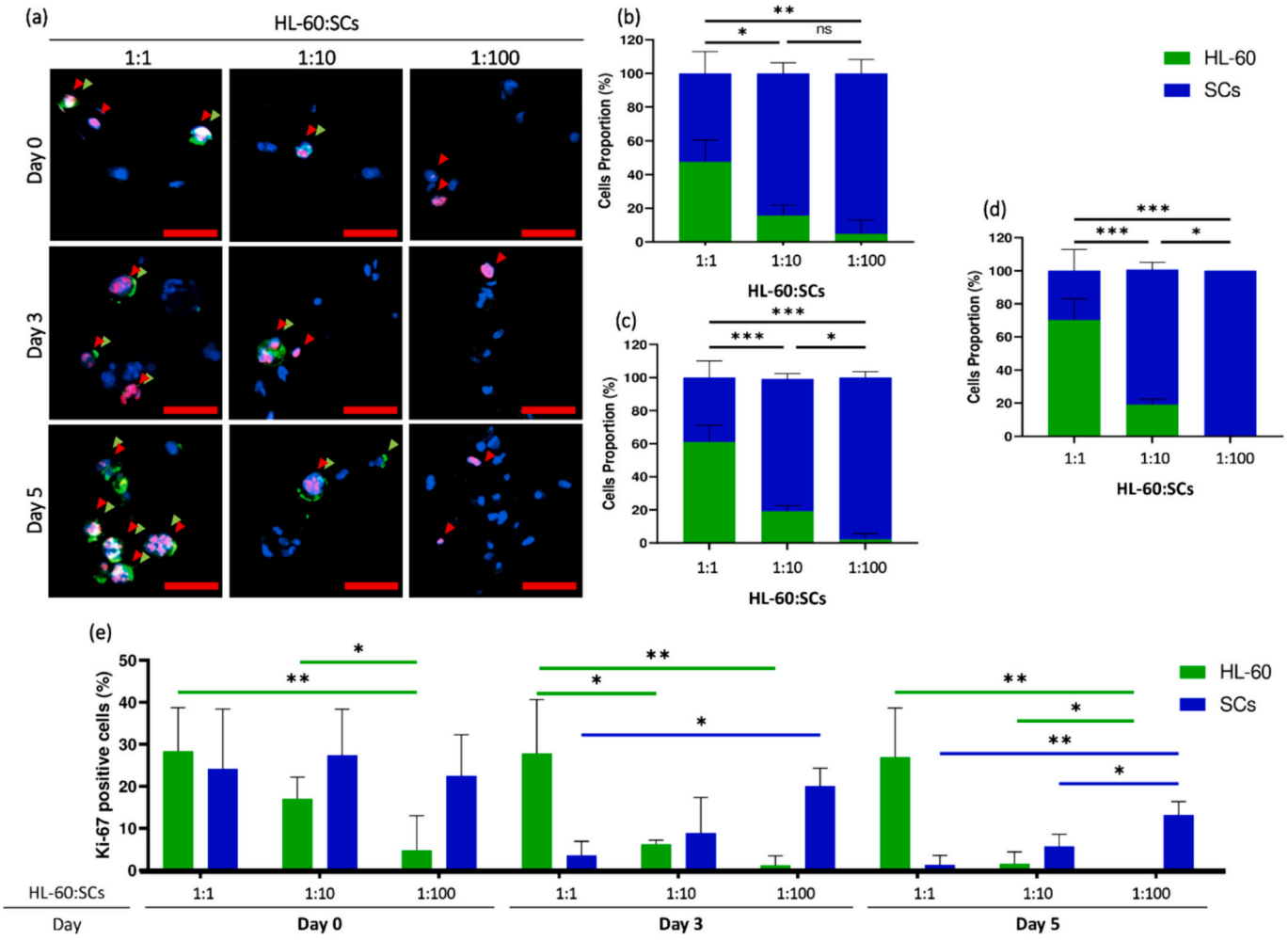

Fig. 5. CD43/Ki67 immunofluorescence (CD43: green/Ki67: red/Hoechst: blue) analysis of TIMs with different ratios of HL-60:SCs (1:1, 1:10, and 1:100) before and 3 or 5 days after culturing (a) (scale bar: 50 μm). Cell proportion evaluation on day 0 (b), Day 3 (c), and Day 5 (d). Quantification of proliferative HL-60 and SCs before culturing and after 3 or 5 days of culturing (e) (ns, no significant; *, $P < 0.05$; **, $P < 0.01$; ***, $P < 0.001$). (For interpretation of the references to colour in this figure legend, the reader is referred to the web version of this article.)

Table 2
Cell density dynamics of HL-60 and SCs after 3 and 5 days of *in vitro* culture.

Combination (Hl-60:SCs)	Cell density dynamics (%)			
	Day 3		Day 5	
	SCs	HL-60	SCs	HL-60
1:1	38.10 ± 26.94	61.11 ± 23.52	42.50 ± 15.41 [a]	79.44 ± 3.42 [b]
1:10	41.43 ± 40.12	55.56 ± 7.86	52.12 ± 29.40	58.33 ± 11.79
1:100	57.18 ± 5.12	–	58.89 ± 6.85	–

The letter in the same row indicates the statistical difference ($p < 0.01$).

Here we observed that bioprinted hydrogels exposed to PBS experienced significant mass loss compared to those in DMEM/F12, likely due to the presence of Ca^{2+} in DMEM/F12, supporting physically crosslinked alginate. Changing the medium during degradation helps in replenishing Ca^{2+} resources. On the other hand, the degradation of PEGylated fibrin in the bioprinted structure may contribute to the accelerated degradation rate of hydrogels in PBS, which the degradation of high concentrations of PEGylated fibrin in PBS due to the ionic interactions between fibrin and PBS was reported previously [12].

In addition to producing viable cells in bioprinted scaffolds, the main aim of our study was to mimic the natural structure of invasive leukemia tumors in healthy tissue. Although acute myeloid leukemia presents a wide range of variations, established cell lines have provided a valuable platform for decades, enabling efficient, repetitive, and economical investigations. Typically referred to as "liquid tumors," these cells are predominantly found in body fluids rather than forming solid tumors [26,27]. However, it is noteworthy that HL-60 cells, with a doubling time of 36–72 h, have demonstrated a propensity to spontaneously form colonies in semi-solid media [28,29]. In this study, it is imperative to finely tune the HL-60:SCs cell ratio to strike a delicate balance: preventing excessive solid tumor formation while ensuring the retention of adequate levels of cancer cells for a relevant model. Our findings revealed that the cell ratio and culture duration significantly influence tumor formation. HL-60 cells within the TIMs exhibited a doubling time of 72 h when cultured with a HL-60:SCs ratio of 1:10. Contrastingly, within the same timeframe, cells in the HL-60:SCs ratio of 1:1 group underwent a tripling in number. Therefore, due to the dramatically accelerated rate of cancer cell growth, the cell density dynamic percentage greatly rose after 5 days of culture. On the contrary, no cancer cells were found in the group with an HL-60:SCs ratio of 1:100 on the fifth day. The group with an HL-60:SCs ratio of 1:10 was more competent to simulate the invasion of leukemia cells into ovarian tissue because its cancer cells could remain detectable after 5 days of *in vitro* culture without any significant change in the cell density and cell density dynamic. Furthermore, cancer cells were evenly distributed

throughout the bioprinted scaffold within this cohort, ensuring they did not grow in clumps and facilitating their identification through random sectioning.

5. Conclusion

In this study, we formulated a bioink using a combination of PEG, fibroin, and alginate to create hydrogels embedded with HL-60 cells and stromal cells, aimed at constructing a suitable 3D tumor microenvironment mimicking acute leukemia cell invasion in ovarian tissue. These 3D bioprinted microtumor models present a promising avenue for accelerating drug development processes. They enable a more precise evaluation of therapeutic effectiveness and facilitate the characterization of *in vitro* cellular behaviors that closely mimic *in vivo* responses. Performing a preliminary drug testing assay would now be valuable to demonstrate the effectiveness of our model compared to responses observed in 2D culture systems.

Funding

This study was supported by grants from the Foundation Louvain (Ph.D. scholarship awarded to S.M., as part of a legacy from Mr. Frans Heyes, and Ph.D. scholarship awarded to A.D. as part of a legacy from Mrs. Ilse Schirmer).

CRediT authorship contribution statement

Saeid Moghassemi: Writing – original draft, Validation, Methodology, Investigation, Formal analysis, Data curation, Conceptualization. **Arezoo Dadashzadeh:** Writing – original draft, Validation, Methodology, Formal analysis, Data curation, Conceptualization. **Christiani A. Amorim:** Writing – review & editing, Resources, Project administration, Funding acquisition.

Declaration of competing interest

The authors declare the following financial interests/personal relationships which may be considered as potential competing interests:

Christiani A. Amorim reports financial support was provided by Louvain Foundation. If there are other authors, they declare that they have no known competing financial interests or personal relationships that could have appeared to influence the work reported in this paper.

Data availability

Data will be made available on request.

Acknowledgments

We thank the Kidney and Pancreatic Transplantation Unit of UCLouvain's Saint-Luc Hospital for donating ovaries for this study. We would like to express our gratitude to Aspect Biosystems for providing us with the opportunity to utilize a microfluidic RX1 Bioprinter and for their support in supplying materials and engaging in scientific communication.

References

[1] I. Matai, G. Kaur, A. Seyedsalehi, A. McClinton, C.T. Laurencin, Progress in 3D bioprinting technology for tissue/organ regenerative engineering, Biomaterials 226 (2020) 119536.
[2] C. Lee, E. Abelseth, L. De La Vega, S. Willerth, Bioprinting a novel glioblastoma tumor model using a fibrin-based bioink for drug screening, Materials Today Chemistry 12 (2019) 78–84.
[3] C.S. Szot, C.F. Buchanan, J.W. Freeman, M.N. Rylander, 3D in vitro bioengineered tumors based on collagen I hydrogels, Biomaterials 32 (2011) 7905–7912.
[4] M.V. Monteiro, V.M. Gaspar, L.P. Ferreira, J.F. Mano, Hydrogel 3D in vitro tumor models for screening cell aggregation mediated drug response, Biomater. Sci. 8 (2020) 1855–1864.
[5] C.A. Amorim, Artificial ovary, in: Gonadal Tissue Cryopreservation in Fertility Preservation, 2016, pp. 175–192.
[6] S. Moghassemi, A. Dadashzadeh, A. Camboni, O. Feron, R.B. Azevedo, C. A. Amorim, Ex vivo purging of cancer cells from ovarian tissue using photodynamic therapy: a novel strategy to restore fertility in leukemia patients, Human Reproduction Open. 2023 (2023) hoad005.
[7] W.H.B. Wallace, R.A. Anderson, D.S. Irvine, Fertility preservation for young patients with cancer: who is at risk and what can be offered? Lancet Oncol. 6 (2005) 209–218.
[8] T. Maltaris, R. Seufert, F. Fischl, M. Schaffrath, K. Pollow, H. Koelbl, R. Dittrich, The effect of cancer treatment on female fertility and strategies for preserving fertility, Eur. J. Obstet. Gynecol. Reprod. Biol. 130 (2007) 148–155.
[9] S. Moghassemi, A. Dadashzadeh, A. Camboni, O. Feron, R.B. Azevedo, C. A. Amorim, Photodynamic therapy using OR141-loaded nanovesicles for eradication of leukemic cells from ovarian tissue, Photodiagnosis Photodyn. Ther. 40 (2022) 103139.
[10] S. Moghassemi, A. Dadashzadeh, P.E.N. de Souza, R.B. Azevedo, C.A. Amorim, AlPc/ZnPc-based oncological photodynamic therapy for a selective eradication of leukemic cells from ovarian tissue, Photodiagnosis Photodyn. Ther. 36 (2021) 102555.
[11] S. Moghassemi, A. Dadashzadeh, R.B. de Azevedo, C.A. Amorim, Secure transplantation by tissue purging using photodynamic therapy to eradicate malignant cells, J. Photochem. Photobiol. B Biol. 234 (2022) 112546.
[12] A. Dadashzadeh, S. Moghassemi, C. Amorim, Evaluation of PEGylated fibrin as a three-dimensional biodegradable scaffold for ovarian tissue engineering, Materials Today Chemistry. 22 (2021) 100626.
[13] A. Dadashzadeh, S. Moghassemi, M. Grubliauskaité, H. Vlieghe, D. Brusa, C. A. Amorim, Medium supplementation can influence the human ovarian cells in vitro, J. Ovarian Res. 15 (2022) 1–12.
[14] C.A. Amorim, M.-M. Dolmans, A. David, J. Jaeger, J. Vanacker, A. Camboni, J. Donnez, A. Van Langendonckt, Vitrification and xenografting of human ovarian tissue, Fertil. Steril. 98 (2012) 1291–1298 (e1292).
[15] C.A. Amorim, A. Van Langendonckt, A. David, M.-M. Dolmans, J. Donnez, Survival of human pre-antral follicles after cryopreservation of ovarian tissue, follicular isolation and in vitro culture in a calcium alginate matrix, Hum. Reprod. 24 (2009) 92–99.
[16] A. Dadashzadeh, S. Moghassemi, C. Amorim, Bioprinting of a liposomal oxygen-releasing scaffold for ovary tissue engineering, Tissue Eng.
[17] H. Jafari, A. Dadashzadeh, S. Moghassemi, P. Zahedi, C.A. Amorim, A. Shavandi, Ovarian cell encapsulation in an enzymatically crosslinked silk-based hydrogel with tunable mechanical properties, Gels 7 (2021) 138.
[18] S. Moghassemi, A. Dadashzadeh, H. Jafari, P. Ghaffari-Bohlouli, A. Shavandi, C. A. Amorim, Liposomal oxygen-generating hydrogel for enhancing cell survival under hypoxia condition, Colloids Surf. B Biointerfaces 231 (2023) 113562.
[19] A. Dadashzadeh, S. Moghassemi, A. Peaucelle, C.M. Lucci, C.A. Amorim, Mind the mechanical strength: tailoring a 3D matrix to encapsulate isolated human preantral follicles, Human Reproduction Open. 2023 (2023) hoad004.
[20] D.E. Kehoe, D. Jing, L.T. Lock, E.S. Tzanakakis, Scalable stirred-suspension bioreactor culture of human pluripotent stem cells, Tissue Eng. Part A 16 (2010) 405–421.
[21] V.K. Lee, G. Dai, H. Zou, S.-S. Yoo, Generation of 3-D glioblastoma-vascular niche using 3-D bioprinting, in: 2015 41st Annual Northeast Biomedical Engineering Conference (Nebec), IEEE 1–2.
[22] Y. Zhao, R. Yao, L. Ouyang, H. Ding, T. Zhang, K. Zhang, S. Cheng, W. Sun, Three-dimensional printing of Hela cells for cervical tumor model in vitro, Biofabrication 6 (2014) 035001.
[23] F. Leonard, B. Godin, 3D in vitro model for breast cancer research using magnetic levitation and bioprinting method, in: Breast Cancer: Methods and Protocols, 2016, pp. 239–251.
[24] S. Bajpai, S. Sharma, Investigation of swelling/degradation behaviour of alginate beads crosslinked with Ca2+ and Ba2+ ions, React. Funct. Polym. 59 (2004) 129–140.
[25] L. De la Vega, D.A. Rosas Gómez, E. Abelseth, L. Abelseth, V. Allisson da Silva, S. M. Willerth, 3D bioprinting human induced pluripotent stem cell-derived neural tissues using a novel lab-on-a-printer technology, Appl. Sci. 8 (2018) 2414.
[26] M. Ohanian, S. Faderl, F. Ravandi, N. Pemmaraju, G. Garcia-Manero, J. Cortes, Z. Estrov, Is acute myeloid leukemia a liquid tumor? Int. J. Cancer 133 (2013) 534–543.
[27] Z. Zhu, K. Hattori, H. Zhang, X. Jimenez, D. Ludwig, S. Dias, P. Kussie, H. Koo, H. Kim, D. Lu, Inhibition of human leukemia in an animal model with human antibodies directed against vascular endothelial growth factor receptor 2. Correlation between antibody affinity and biological activity, Leukemia 17 (2003) 604–611.
[28] B.L. Spangelo, M. Pompilius, D.D. Farrimond, N. Stevens, R. Nieva, S. Shroff, M. Badamchian, C.R. Johnson, W.D. Jarvis, Presence of a peptide component of thymosin fraction-5 manifesting discrete cytostatic properties in HL-60 human promyelocytic leukemia cells, Int. Immunopharmacol. 5 (2005) 1317–1329.
[29] R. Skopek, M. Palusińska, K. Kaczor-Keller, R. Pingwara, A. Papierniak-Wygładała, T. Schenk, S. Lewicki, A. Zelent, Ł. Szymański, Choosing the right cell line for acute myeloid leukemia (AML) research, Int. J. Mol. Sci. 24 (2023) 5377.